magnetochemistry

MDPI

Supplementary Materials: Effect of the Alkaline Metal Ion on the Crystal Structure and Magnetic Properties of Heterometallic Gd^{III}-V^{IV} Complexes Based on Cyclobutane-1,1-Dicarboxylate Anions

Evgeniya S. Bazhina [1,*], Alexander A. Korlyukov [2], Julia K. Voronina [1], Konstantin A. Babeshkin [1], Elena A. Ugolkova [1], Nikolay N. Efimov [1], Matvey V. Fedin [3], Mikhail A. Kiskin [1,*] and Igor L. Eremenko [1,2]

[1] N.S. Kurnakov Institute of General and Inorganic Chemistry of the Russian Academy of Sciences, Leninskiy prosp. 31, 119991 Moscow, Russia; juliavoronina@mail.ru (J.K.V.); bkonstantan@yandex.ru (K.A.B.); tipperiri@yandex.ru (E.A.U.); nnefimov@yandex.ru (N.N.E.); ilerem@igic.ras.ru (I.L.E.)

[2] A.N. Nesmeyanov Institute of Organoelement Compounds of the Russian Academy of Sciences, Vavilova str. 28, 119991 Moscow, Russia; alex@xrlab.ineos.ac.ru

[3] International Tomography Center of the Siberian Branch of the Russian Academy of Sciences, Institutskaya str. 3a, 630090 Novosibirsk, Russia; mfedin@tomo.nsc.ru

* Correspondence: evgenia-vo@mail.ru (E.S.B.); mkiskin@igic.ras.ru (M.A.K.)

S-I. Crystal structure description

Table S1. Selected bond lengths *d* (Å) and angles *ω* (°) for **1**.

Bond	*d*	Bond	*d*
V1–O5	1.5968(19)	Gd1–O12$^{(i)}$	2.3997(18)
V1–O4	1.9632(17)	Gd1–O11	2.4092(18)
V1–O3	1.9754(17)	Gd1–O11$^{(i)}$	2.4093(18)
V1–O1	1.9906(17)	Na1–O6	2.4170(19)
V1–O2	2.0208(17)	Na1–O6$^{(ii)}$	2.4170(19)
V1–O6	2.2995(18)	Na1–O14	2.445(2)
Gd1–O13	2.3723(17)	Na1–O14$^{(ii)}$	2.445(2)
Gd1–O13$^{(i)}$	2.3723(17)	Na1–O3	2.5359(17)
Gd1–O7	2.3785(17)	Na1–O3$^{(ii)}$	2.5358(17)
Gd1–O7$^{(i)}$	2.3785(17)	Na1–O1	2.631(2)
Gd1–O12	2.3996(18)	Na1–O1$^{(ii)}$	2.631(2)

Angle	*ω*	Angle	*ω*
O5–V1–O4	101.17(9)	O13–Gd1–O12	149.67(6)
O5–V1–O3	99.83(8)	O7–Gd1–O12	90.69(6)
O4–V1–O3	89.33(7)	O7$^{(i)}$–Gd1–O12	101.97(6)
O5–V1–O1	101.69(9)	O13$^{(i)}$–Gd1–O12$^{(i)}$	149.67(6)
O4–V1–O1	157.10(8)	O13–Gd1–O12$^{(i)}$	71.56(6)
O3–V1–O1	85.60(7)	O7–Gd1–O12$^{(i)}$	101.97(6)
O5–V1–O2	100.21(8)	O7$^{(i)}$–Gd1–O12$^{(i)}$	90.69(6)
O4–V1–O2	90.27(7)	O12–Gd1–O12$^{(i)}$	138.67(9)
O3–V1–O2	159.65(7)	O13$^{(i)}$–Gd1–O11	119.89(6)
O1–V1–O2	86.89(7)	O13–Gd1–O11	131.58(6)
O5–V1–O6	177.80(9)	O7–Gd1–O11	147.67(6)
O4–V1–O6	79.87(7)	O7$^{(i)}$–Gd1–O11	67.73(6)
O3–V1–O6	78.21(7)	O12–Gd1–O11	70.10(6)
O1–V1–O6	77.24(7)	O12$^{(i)}$–Gd1–O11	79.12(7)

O2–V1–O6	81.69(7)	O13i–Gd1–O11(i)	131.58(6)
O13(i)–Gd1–O13	78.41(9)	O13–Gd1–O11(i)	119.89(6)
O13(i)–Gd1–O7	74.86(6)	O7–Gd1–O11(i)	67.73(6)
O13–Gd1–O7	77.26(6)	O7(i)–Gd1–O11(i)	147.67(6)
O13(i)–Gd1–O7(i)	77.26(6)	O12–Gd1–O11(i)	79.12(7)
O13–Gd1–O7(i)	74.86(6)	O12(i)–Gd1–O11(i)	70.10(6)
O7–Gd1–O7(i)	143.79(8)	O11–Gd1–O11(i)	82.86(9)
O13(i)–Gd1–O12	71.56(6)		

Symmetry codes: (i) –x+1, y, –z+1/2; (ii) –x, y, –z+1/2.

Table S2. Selected bond lengths *d* (Å) and angles *ω* (°) for **2**.

Bond	***d***	**Bond**	***d***
V1–O1	1.589(3)	Gd1–O13W	2.450(2)
V1–O2	2.001(2)	Gd1–O15	2.821(2)
V1–O3	2.009(2)	Gd1–O18	2.454(2)
V1–O4W	2.238(2)	Rb1–O3(i)	3.060(2)
V1–O6	2.010(2)	Rb1–O3W	3.477(2)
V1–O7	2.019(2)	Rb1–O7(i)	2.981(2)
V2–O3W	2.417(2)	Rb1–O8W(ii)	3.144(2)
V2–O10	1.990(2)	Rb1–O10	3.371(2)
V2–O11	2.001(2)	Rb1–O11W	3.499(3)
V2–O14	1.584(2)	Rb1–O12	2.908(2)
V2–O15	2.016(2)	Rb1–O12W	2.845(2)
V2–O16	1.984(2)	Rb1–O13(iii)	2.843(2)
Gd1–O5	2.363(2)	Rb1–O13W	3.002(2)
Gd1–O6W	2.491(2)	O3–Rb1(iv)	3.060(2)
Gd1–O7W	2.331(2)	O7–Rb1(iv)	2.981(2)
Gd1–O8W	2.473(2)	O8W–Rb1(ii)	3.144(2)
Gd1–O9W	2.390(2)	O13–Rb1(iii)	2.843(2)
Gd1–O10W	2.379(2)		

Angle	***ω***	**Angle**	***ω***
O1–V1–O2	100.60(11)	O5–Gd1–O10W	77.37(8)
O1–V1–O3	99.59(11)	O5–Gd1–O13W	129.85(8)
O1–V1–O4W	178.76(12)	O5–Gd1–O15	69.67(7)
O1–V1–O6	99.92(11)	O5–Gd1–O18	79.73(7)
O1–V1–O7	98.83(11)	O6W–Gd1–O15	106.13(7)
O2–V1–O3	87.07(9)	O7W–Gd1–O5	137.66(8)
O2–V1–O4W	79.88(9)	O7W–Gd1–O6W	69.47(8)
O2–V1–O6	88.00(9)	O7W–Gd1–O8W	68.03(8)
O2–V1–O7	160.51(10)	O7W–Gd1–O9W	96.61(9)
O3–V1–O4W	79.28(10)	O7W–Gd1–O10W	85.14(9)
O3–V1–O6	160.44(10)	O7W–Gd1–O13W	79.34(8)
O3–V1–O7	91.20(9)	O7W–Gd1–O15	141.62(8)
O6–V1–O4W	81.23(9)	O7W–Gd1–O18	140.35(8)
O6–V1–O7	87.19(9)	O8W–Gd1–O6W	120.27(8)
O7–V1–O4W	80.72(9)	O8W–Gd1–O15	133.14(7)
O10–V2–O3W	78.25(9)	O9W–Gd1–O6W	69.89(8)
O10–V2–O11	86.70(9)	O9W–Gd1–O8W	75.48(8)

O10–V2–O15	86.82(9)	O9W–Gd1–O13W	140.28(8)
O11–V2–O3W	81.66(9)	O9W–Gd1–O15	118.21(7)
O11–V2–O15	158.56(10)	O9W–Gd1–O18	75.35(8)
O14–V2–O3W	176.07(11)	O10W–Gd1–O6W	140.19(8)
O14–V2–O10	103.63(11)	O10W–Gd1–O8W	73.57(8)
O14–V2–O11	101.82(11)	O10W–Gd1–O9W	145.76(8)
O14–V2–O15	99.56(11)	O10W–Gd1–O13W	73.77(8)
O14–V2–O16	102.08(11)	O10W–Gd1–O15	75.11(7)
O15–V2–O3W	77.02(9)	O10W–Gd1–O18	123.22(8)
O16–V2–O3W	75.97(9)	O13W–Gd1–O6W	71.80(8)
O16–V2–O10	154.22(10)	O13W–Gd1–O8W	135.13(8)
O16–V2–O11	89.94(9)	O13W–Gd1–O15	63.78(7)
O16–V2–O15	87.08(9)	O13W–Gd1–O18	82.97(8)
O5–Gd1–O6W	141.46(8)	O18–Gd1–O6W	71.36(8)
O5–Gd1–O8W	70.10(8)	O18–Gd1–O8W	141.34(7)
O5–Gd1–O9W	78.66(8)	O18–Gd1–O15	48.23(7)

Symmetry codes: (i) x–1/2, y+1/2, z; (ii) –x+1, –y+2, –z+1; (iii) –x+1, y, –z+3/2; (iv) x+1/2, y–1/2, z.

Table S3. Selected bond lengths *d* (Å) and angles *ω* (°) for **3**.

Bond	***d***	**Bond**	***d***
V1–O8	2.005 (3)	Gd1–O16	2.414 (3)
V1–O16W	2.251 (4)	Gd1–O13W	2.422 (3)
V1–O2	1.997 (3)	Gd1–O12W	2.422 (4)
V1–O4	1.994 (3)	Gd1–O4W	2.383 (4)
V1–O6	2.002 (3)	Gd1–O1W	2.465 (4)
V1–O1	1.589 (4)	Cs1–O13i	3.478 (4)
V2–O14	1.998 (3)	Cs1–O8	3.313 (3)
V2–O11W	2.369 (4)	Cs1–O5	3.611 (4)
V2–O11	2.002 (4)	Cs1–O16W	3.163 (4)
V2–O15	2.017 (3)	Cs1–O14W	3.470 (4)
V2–O17	1.983 (4)	Cs1–O12	3.163 (4)
V2–O10	1.581 (4)	Cs1–O4	3.111 (3)
Gd1–O15	2.732 (3)	Cs1–O9W	3.409 (4)
Gd1–O2W	2.478 (3)	Cs1–O13W	3.250 (3)
Gd1–O9	2.326 (3)	Cs1–O15W	3.301 (4)
Gd1–O5W	2.455 (4)		

Angle	***ω***	**Angle**	***ω***
O8–V1–O16W	77.38(14)	O9–Gd1–O5W	75.96(12)
O2–V1–O8	156.21(15)	O9–Gd1–O16	84.64(12)
O2–V1–O16W	79.39(14)	O9–Gd1–O13W	77.33(12)
O2–V1–O6	84.52(14)	O9–Gd1–O12W	129.36(12)
O4–V1–O8	90.51(14)	O9–Gd1–O4W	75.48(12)
O4–V1–O16W	77.93(14)	O9–Gd1–O1W	142.86(12)
O4–V1–O2	89.58(14)	O5W–Gd1–O15	139.43(11)
O4–V1–O6	161.49(15)	O5W–Gd1–O2W	112.45(12)
O6–V1–O8	87.94(14)	O5W–Gd1–O1W	68.58(12)
O6–V1–O16W	83.73(14)	O16–Gd1–O15	49.50(11)
O1–V1–O8	102.59(17)	O16–Gd1–O2W	66.14(12)

O1–V1–O16W	178.16(18)	O16–Gd1–O5W	146.86(12)
O1–V1–O2	100.81(17)	O16–Gd1–O13W	124.66(12)
O1–V1–O4	100.24(17)	O16–Gd1–O12W	80.32(12)
O1–V1–O6	98.10(18)	O16–Gd1–O1W	131.85(12)
O14–V2–O11W	82.48(14)	O13W–Gd1–O15	75.22(11)
O14–V2–O11	87.23(14)	O13W–Gd1–O2W	144.23(12)
O14–V2–O15	161.38(15)	O13W–Gd1–O5W	77.18(12)
O11–V2–O11W	79.24(14)	O13W–Gd1–O12W	72.62(12)
O11–V2–O15	87.62(14)	O13W–Gd1–O1W	84.29(12)
O15–V2–O11W	78.99(13)	O12W–Gd1–O15	64.09(11)
O17–V2–O14	89.77(14)	O12W–Gd1–O2W	76.75(12)
O17–V2–O11W	76.08(14)	O12W–Gd1–O5W	132.64(12)
O17–V2–O11	155.31(15)	O12W–Gd1–O1W	72.82(12)
O17–V2–O15	87.47(14)	O4W–Gd1–O15	118.80(11)
O10–V2–O14	100.54(17)	O4W–Gd1–O2W	69.95(12)
O10–V2–O11W	175.26(16)	O4W–Gd1–O5W	69.96(12)
O10–V2–O11	104.47(17)	O4W–Gd1–O16	79.37(12)
O10–V2–O15	98.07(17)	O4W–Gd1–O13W	141.35(12)
O10–V2–O17	100.17(17)	O4W–Gd1–O12W	145.81(12)
O2W–Gd1–O15	107.35(11)	O4W–Gd1–O1W	101.55(12)
O9–Gd1–O15	69.41(11)	O1W–Gd1–O15	136.02(11)
O9–Gd1–O2W	137.84(12)	O1W–Gd1–O2W	69.20(12)

Symmetry codes: (i) –x+2, –y+2, –z+1.

Table S4. Continuous shape measures (CShM) for GdO_8 coordination polyhedra in compounds **1-3**. The lowest SHAPE values are shown highlighted indicating best fits.

Structure ML_8	SAPR-8	TDD-8	JBTPR-8	BTPR-8	JSD-8
1	1.610	**0.661**	3.174	2.563	3.920
2	1.021	1.941	1.391	**0.681**	3.734
3	**0.760**	1.841	2.264	1.371	4.711

Codes: SAPR-8 (D4d) Square antiprism; TDD-8 (D2d) Triangular dodecahedron; JBTPR-8 (C2v) Biaugmented trigonal prism J50; BTPR-8 (C2v) Biaugmented trigonal prism; JSD-8 (D2d) Snub diphenoid J84.

Table S5. Hydrogen bonding parameters of structure **1**.

Fragment D–H···A	Distance/ Å			D–H···A /°
	D–H	H···A	D···A	
O11–H11···O7(i)	0.91	2.35	2.668(3)	100
O11–H11'···O14(ii)	0.90	1.76	2.628(3)	161
O12–H12···O9(ii)	0.87	1.93	2.787(3)	168
O12–H12'···O5(iii)	0.84	1.93	2.759(3)	171
O13–H13···O8(iv)	0.83	1.88	2.697(3)	172
O13–H13'···O2(i)	0.82	2.00	2.716(3)	146
O14–H14···O3(iv)	0.95	2.42	3.099(3)	128
O14–H14···O9(iv)	0.95	2.00	2.815(3)	143
O14–H14'···O10(i)	0.95	1.82	2.714(3)	156
O6–H61···O8(iv)	0.95	1.82	2.733(3)	160
O6–H62···O10(i)	0.95	1.85	2.765(3)	161
C6–H6A···O8	0.99	2.48	2.846(4)	101

C6–H6B...O7	0.99	2.41	2.795(3)	102
C10–H10B···O9(v)	0.99	2.60	3.456(3)	145
C12–H12B···O10	0.99	2.47	2.846(3)	102

Symmetry codes: (i) 1–x, y, 1/2–z; (ii) 1/2+x, 1/2+y, z; (iii) 1–x, 1–y, 1–z; (iv) –x, y, 1/2–z; (v) 1/2-x, 1/2–y, 1–z.

Table S6. Hydrogen bonding parameters of structure **2**.

Fragment D–H···A	Distance/ Å			D–H···A /°
	D–H	H···A	D···A	
O4W–H4WB···O5W	0.85	1.94	2.785(3)	174.0
O9W–H9WA···O5W	0.85	1.83	2.643(3)	158.9
O10W–H10B···O10	0.85	1.89	2.729(3)	170.7
O13W–H13B···O3W	0.85	2.00	2.852(3)	175.9
O2W–H2W···O17	0.85	1.92	2.758(4)	167.3
O5W–H5WA···O1W	0.85	2.14	2.849(4)	140.7

Table S7. Hydrogen bonding parameters of structure **3**.

Fragment D–H···A	Distance/ Å			D–H···A /°
	D–H	H···A	D···A	
O6W–H6WA···O7(i)	0.85	1.81	2.629 (5)	161.0
O6W–H6WB···O10W(ii)	0.85	1.83	2.672 (5)	170.4
O16W–H16A···O6W	0.85	1.81	2.653 (5)	168.6
O16W–H16B···O3(iii)	0.85	1.83	2.658 (5)	163.6
O2W–H2WA···O10W(iv)	0.85	1.87	2.704 (5)	168.9
O2W–H2WB···O8W(v)	0.85	2.07	2.872 (5)	158.1
O14W–H14A···O7W	0.85	1.96	2.781 (5)	161.1
O14W–H14B···O2W(vi)	0.85	2.13	2.897 (5)	149.3
O10W–H10C···O18	0.85	1.86	2.675 (5)	161.5
O10W–H10D···O9W(vii)	0.85	1.94	2.786 (5)	173.3
O5W–H5WA···O6W	0.85	1.84	2.662 (5)	163.6
O5W–H5WB···O14W	0.85	1.89	2.736 (5)	170.9
O3W–H3WA···O2(i)	0.85	2.03	2.879 (5)	176.9
O3W–H3WB···O5(v)	0.85	2.00	2.773 (5)	150.8
O7W–H7WA···O13(vii)	0.85	1.96	2.742 (5)	152.0
O7W–H7WB···O6(viii)	0.85	2.06	2.895 (5)	168.6
O9W–H9WA···O15W(ix)	0.85	1.90	2.734 (5)	168.9
O9W–H9WB···O14(vii)	0.85	2.02	2.826 (5)	157.9
O13W–H13A···O13(vii)	0.85	2.07	2.809 (5)	144.6
O13W–H13B···O11	0.85	1.86	2.704 (5)	175.5
O12W–H12B···O18(iv)	0.85	1.86	2.703 (5)	168.5
O4W–H4WA···O7(i)	0.85	1.95	2.799 (5)	177.5
O4W–H4WB···O3W	0.85	1.81	2.646 (5)	168.8
O1W–H1WA···O7W	0.85	1.93	2.744 (5)	160.4
O15W–H15B···O3(iii)	0.85	1.98	2.796 (5)	160.2
O8W–H8WA···O5	0.85	1.92	2.744 (5)	162.2
O8W–H8WB···O9W	0.85	1.93	2.779 (5)	173.6
O11W–H11A···O8W(vii)	0.98 (2)	1.85 (2)	2.821 (5)	170 (6)
O11W–H11B···O12(vii)	0.98 (2)	1.93 (5)	2.753 (5)	140 (6)

Symmetry codes: (i) –x+1, –y+1, –z; (ii) x, y, z–1; (iii) –x+1, –y+2, –z; (iv) –x+2, –y+1, –z+1; (v) x, y–1, z; (vi) –x+2, –y+1, –z; (vii) –x+2, –y+2, –z+1; (viii) x+1, y, z; (ix) –x+2, –y+2, -z.

S-II. EPR Spectroscopy

Figure S1. shows a rough simulation of the X-band and Q-band EPR spectra of 1 at 80 K. The use of D~0.08 cm^{-1} and E/D~0.1-0.15 yields qualitatively reasonable agreement; although simulations do not exactly reproduce all the spectral features, they certainly reproduce correctly the width of the spectra, which is mainly determined by D. The g-value of g = 2 was taken for Gd^{III}, which is typical of this ion.

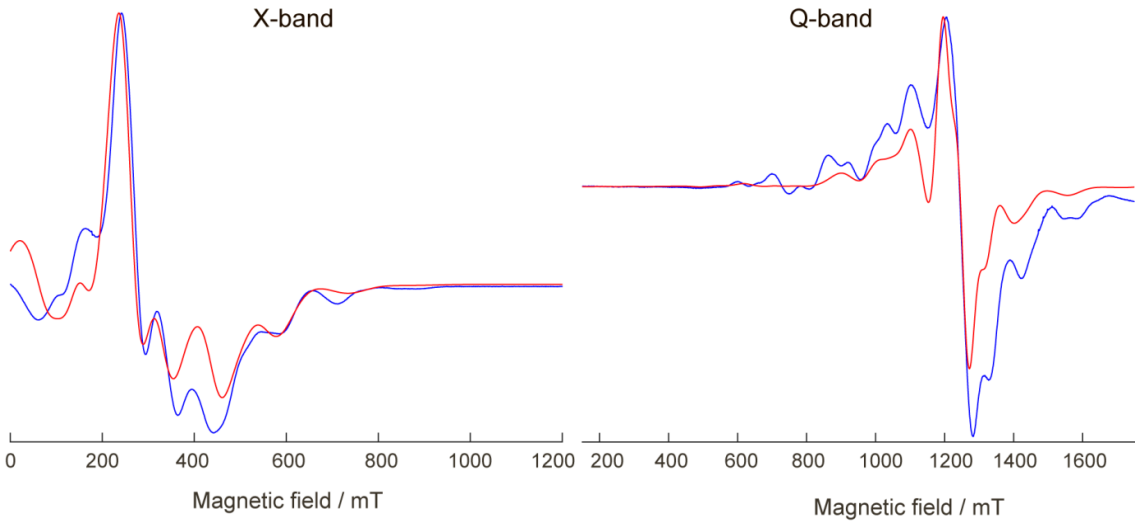

Figure S1. X-band (left) and Q-band (right) EPR spectra of **1** at T = 80 K. Experiment (blue) and simulation using the parameters given in the text (red).

Figure S2 simulates the anticipated contributions of Gd^{III} S = 7/2 ion and two V^{IV} S = 1/2 ions into the overall EPR spectrum. The above parameters of ZFS and g = 2 were taken for Gd^{III}. For V^{IV} ions, the data for an isostructural compound with diamagnetic Y^{III} instead of Gd^{III} was used as an estimate, namely: g = [1.98 1.98 1.94], A = [190 190 530] MHz (hyperfine interaction tensor) [S1]. It is evident that the contribution of V^{IV} ions (green) is small compared to that of Gd^{III} (blue), and, given the appreciable dipolar V-Gd-V broadening, can be indistinguishable in the overall spectrum (red).

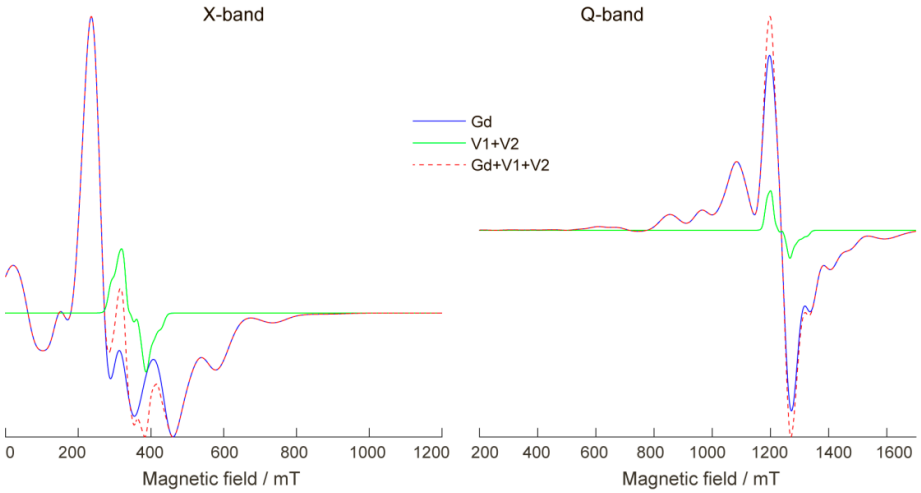

Figure S2. Simulations of X-band (left) and Q-band (right) EPR spectra of Gd^{III} ion, two V^{IV} ions and V^{IV}-Gd^{III}-V^{IV} triad with negligible exchange couplings. See the text for the parameters. The contribution of Gd^{III} is shown in blue, the contribution of two V^{IV} ions is shown in green, and their superposition is given in red. All the spectra are shown on the same scale without individual normalizations.

S-III. Magnetic measurements

DC magnetic measurements

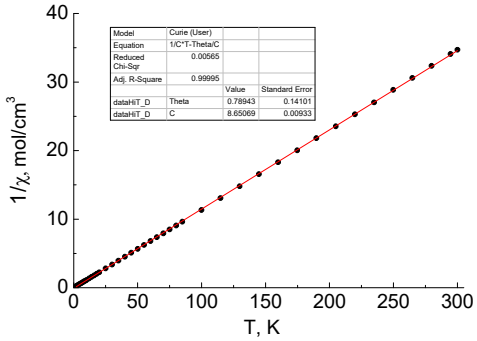

Figure S3. Temperature dependences of 1/χ for **1** (H = 5000 Oe). Red line represents the Curie-Weiss approximation.

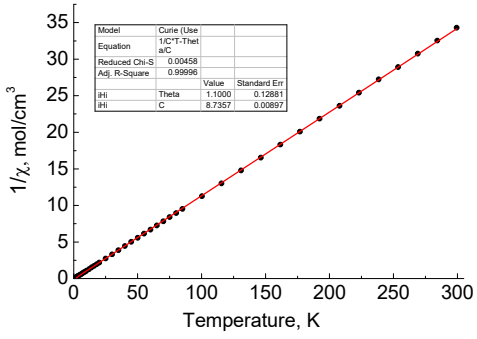

Figure S4. Temperature dependences of 1/χ for **2** (H = 5000 Oe). Red line represents the Curie-Weiss approximation.

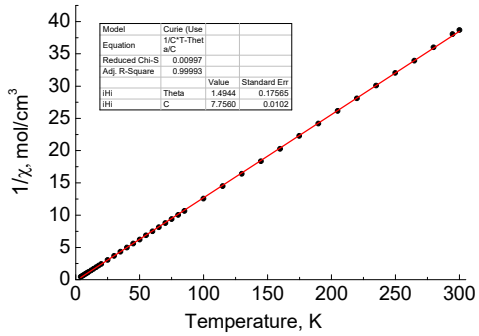

Figure S5. Temperature dependences of 1/χ for **3** (H = 5000 Oe). Red line represents the Curie-Weiss approximation.

All of the fitting of the dc-magnetic properties was made by the use of PHI [S2].At first, we tried to improve the approximations of **1**-**3** with the temperature-independent paramagnetism parameter as a variable (Table S8, Figure S6). The magnetic interactions in **1** was considered as sum of Gd···V (J_1) and general intermolecular (z*J*) exchange. In case of complexes **2** and **3** two different Gd···V exchange interactions can be used for two different V^{IV} ions. However, for **1** the V^{IV} ions are identical, so only one Gd-V exchange parameter can be used. Because of the shape of the experimental dependence, only one variable is not enough to make a successful approximation. The inclusion of the z*J* parameter in the approximation significantly improved the accordance to the experimental data for **1**.

Table S8. Exchange parameters from the PHI fits of **1**-**3** with and without temperature-independent paramagnetism (TIP) as a variable, D = 0, E = 0.

Complex	J_1	J_2	TIP	Residuals, %
1	0.065 ± 0.008	0.065 ± 0.008	-	98.99514
1$_{TIP}$	0.065 ± 0.006	0.065 ± 0.006	$3\cdot10^{-4}$ ± **$9\cdot10^{-4}$**	99.99993
2	-0.089 ± 0.008	0.99 ± 0.03	-	98.32253
2$_{TIP}$	-0.087 ± 0.007	0.97 ± 0.03	$2.3\cdot10^{-3}$ ± $6\cdot10^{-4}$	97.67681
3	-0.050 ± 0.004	0.656 ± 0.009	-	99.66439
3$_{TIP}$	-0.049 ± 0.003	0.651± 0.008	$9\cdot10^{-4}$ ± $2\cdot10^{-4}$	99.72609

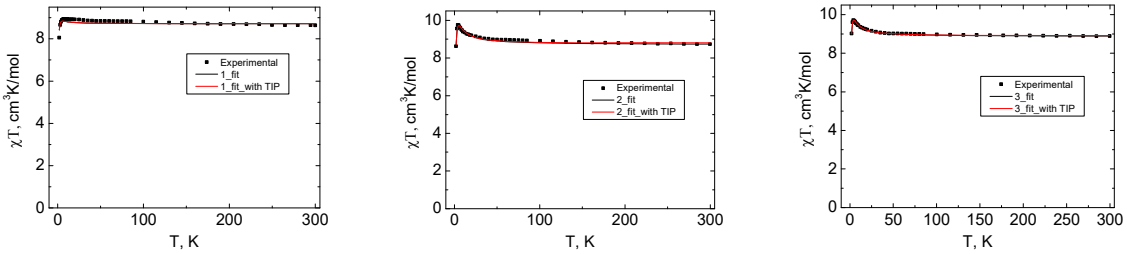

Figure S6. Temperature dependences of $\chi_M T$ for **1**-**3**. The lines are approximations by PHI without (black lines) and with (red lines) the contribution of TIP.

To evaluate the effect of the zero-field splitting tensor on the magnetic properties, the approximations of $\chi_M T(T)$ dependences with D = 0 and E = 0 has been obtained. The fitting parameters for D = 0, E = 0 case are given in Table S9. Using the calculated parameters of the isotropic Hamiltonian, the $\chi_M T(T)$ dependences were simulated taking into

account the ZFS tensor. Since, in this case, only the |D| module can be calculated when determining the ZFS parameters from the EPR spectrum, the following parameters were used: D = ±0.08 cm^{-1}, E = 0.008 cm^{-1} и D = ±0.08 cm^{-1}, E = 0.012 cm^{-1}. The calculation results were averaged over the orientations of the molecule using the Zaremba-Conroy-Wolfsberg (ZCW=5, at ZCW>5 the same results were obtained) integration for all cases of non-zero D, E values.

Table S9. Exchange parameters from the PHI fits of **1**-**3**, D = 0, E = 0.

Complex	J_1	J_2	zJ	Residuals, %
1	0.30 ± 0.01	0.30 ± 0.01	-0.0121 ± 0.0006	99.695
2	-0.089 ± 0.008	0.99 ± 0.03	-	98.323
3	-0.050 ± 0.004	0.656 ± 0.009	-	99.664

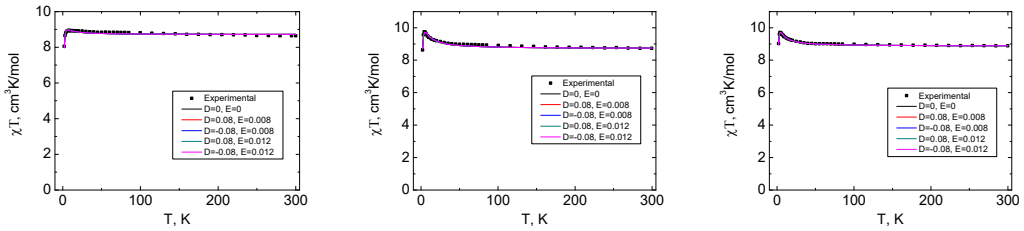

Figure S7. Temperature dependences of $\chi_M T$ for **1**-**3**. The lines represent the PHI approximation for D = 0, E = 0 and simulations for the different values of D and E. TIP correction was not used.

As can be seen from the figure, the influence of the ZFS tensor for all complexes on the magnetic susceptibility is vanishingly small. The Table S10 below shows the $\chi_M T$ (cm^3K/mol) values for the minimum temperature (2 K) for different magnitudes of the ZFS tensor parameters.

Table S10. The values of $\chi_M T$ at 2 K at different values of ZFS tensor.

Complex.	Experimental data	D = 0, E = 0	D = 0.08 cm^{-1}, E = 0.008 cm^{-1}	D = -0.08 cm^{-1}, E = 0.008 cm^{-1}	D = 0.08 cm^{-1}, E = 0.012 cm^{-1}	D = -0.08 cm^{-1}, E = 0.012 cm^{-1}
1	8.053	7.984	7.973	7.975	7.972	7.975
2	8.629	8.700	8.701	8.705	8.700	8.704
3	9.027	9.011	8.986	8.981	8.984	8.980

Thus, the parameters of the ZFS tensor in this case are too small to be taken into account when calculating the magnetic susceptibility. The parameters of the ZFS tensor noticeably affect the approximation of the magnetic susceptibility for orbitally degenerate ions. One of the consequences of orbital degeneracy appears to be the existence of an EPR spectrum only at helium temperatures. Since in our case the EPR spectra were observed at the temperature of liquid nitrogen and at room temperature, we subsequently restrict ourselves to isotropic exchanges.

For complexes **2** and **3** all of the different combinations of the starting exchange values ($J_1 < 0$, $J_2 < 0$; $J_1 > 0$, $J_2 < 0$; $J_1 < 0$, $J_2 > 0$; $J_1 > 0$, $J_2 > 0$; $J_1 = 0$, $J_2 = 0$) always led to the same results. For **1**, however, the second solution was found under the negative initial values of J and positive initial values of zJ. The ZCW = 5 value was fixed for all non-zero D, E values.

Table S11. Exchange parameters from the PHI fits of **1** with different values of D and E.

First solution	$J_1 = J_2 > 0$	zJ < 0	Residuals

D = 0, E = 0	0.298 ± 0.013	-0.012 ± 0.001	99.450
D = 0.08, E = 0.008	0.294 ± 0.014	-0.0118 ± 0.0006	99.449
D = -0.08, E = 0.008	0.292 ± 0.014	-0.0118 ± 0.0006	99.445
D = 0.08, E = 0.012	0.293 ± 0.014	-0.0118 ± 0.0006	99.449
D = -0.08, E = 0.012	0.292 ± 0.014	-0.0118 ± 0.0006	99.445
Second solution	**J_1=J_2 < 0**	**zJ > 0**	**Residuals**
D = 0, E = 0	-0.350 ± 0.019	0.038 ± 0.002	99.584
D = 0.08, E = 0.008	-0.354 ± 0.019	0.038 ± 0.002	99.979
D = -0.08, E = 0.008	-0.354 ± 0.019	0.038 ± 0.002	99.604
D = 0.08, E = 0.012	-0.354 ± 0.019	0.038 ± 0.002	99.092
D = -0.08, E = 0.012	-0.354 ± 0.019	0.038 ± 0.002	99.605

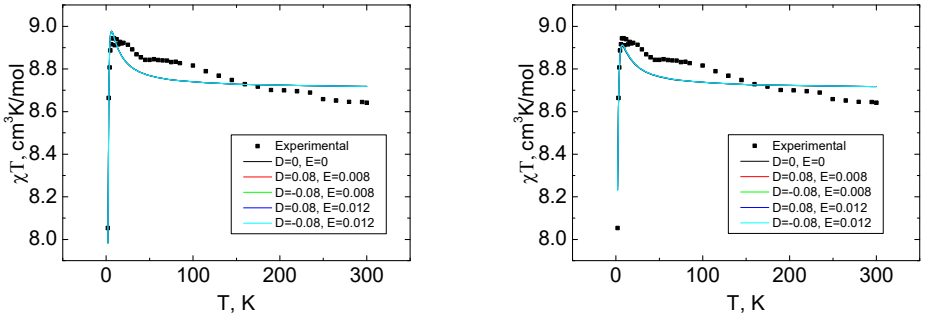

Figure S8. Temperature dependence of $\chi_M T$ for **1**. The lines represent the PHI approximations for the different values of D and E (left – first solution $J_1 = J_2 > 0$ and zJ < 0, right – second solution J_1=J_2 < 0 and zJ > 0).

Table S12. Exchange parameters from the PHI fits of **2** with different values of D and E.

D, E	**J_1**	**J_2**	**Residuals**
D = 0, E = 0	-0.089 ± 0.008	0.989 ± 0.028	98.323
D = 0.08, E = 0.008	-0.083 ± 0.008	0.981 ± 0.028	99.790
D = -0.08, E = 0.008	-0.084 ± 0.008	0.979 ± 0.028	99.293
D = 0.08, E = 0.012	-0.083 ± 0.008	0.981 ± 0.028	99.354
D = -0.08, E = 0.012	-0.084 ± 0.008	0.979 ± 0.028	99.166

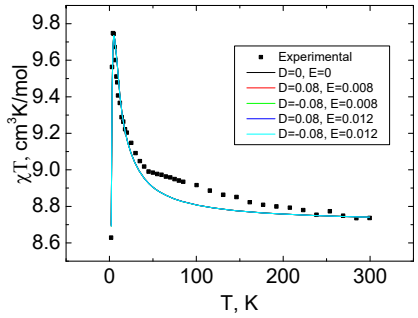

Figure S9. Temperature dependence of $\chi_M T$ for **2**. The lines represent the PHI approximations for the different values of D and E.

Table S13. Exchange parameters from the PHI fits of **3** with different values of D and E.

D, E	**J_1**	**J_2**	**Residuals**
D = 0, E = 0	-0.050 ± 0.004	0.656 ± 0.009	99.664

D = 0.08, E = 0.008	-0.043 ± 0.004	0.648 ± 0.009	99.613
D = -0.08, E = 0.008	-0.044 ± 0.004	0.646 ± 0.009	98.998
D = 0.08, E = 0.012	-0.043 ± 0.004	0.648 ± 0.009	99.001
D = -0.08, E = 0.012	-0.044 ± 0.004	0.646 ± 0.009	99.957

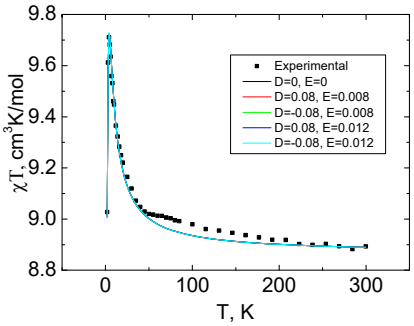

Figure S10. Temperature dependence of $\chi_M T$ for **3**. The lines represent the PHI approximations for the different values of D and E.

The results of the approximation of χ_MT(T) for **1**-**3**.

The interpretation of the experimental plots $\chi_M T$ vs. T for compounds **2** and **3** was carried out in terms of the isotropic spin-Hamiltonian (SH) for a Gd^{III} ion (S_{Gd} = 7/2) interacting with two V^{IV} ions (S_V= 1/2):

$$H_{2,3} = -2J_1 S_{Gd} S_{V_1} - 2J_2 S_{Gd} S_{V_2} + g\beta H(S_{Gd} + S_{V_1} + S_{V_2}) \quad (1)$$

where J_1 and J_2 are the parameters corresponding to the V···Gd exchange couplings, S_{V1} and S_{V2} are the spin operators of two V^{IV} ions (V1 and V2 in accordance with the structure numbering), and S_{Gd} is the spin operator of Gd^{III}. The parameter of isotropic exchange between vanadium ions was taken to be zero for compounds **2** and **3**. The best fit of the experimental data of $\chi_M T$ *vs.* T for **2** and **3** was achieved with the following SH parameters: J_1 = 0.989±0.028 cm^{-1}, J_2 = −0.089±0.008 cm^{-1}, g = 2.01 for **2** and J_1 = 0.656±0.009 cm^{-1}, J_2 = −0.04980±0.00365 cm^{-1}, g = 2.03 for **3**.

For the interpretation of the temperature dependence of $\chi_M T$ for complex **1**, in addition to considering the magnetic exchange between Gd^{III} and V^{IV} ions (J_1), it is also necessary to take into account the exchange between V^{IV} ions belonging to neighbouring {GdV_2} units (J_2), i.e. it is necessary to solve the SH of the linear chain:

$$H_1 = \sum_i \left(-2J_1(S^i_{Gd}S^i_{V_1} + S^i_{Gd}S^i_{V_2}) - 2J_2(S^{i-1}_{V_1}S^i_{V_2} + S^i_{V_1}S^{i+1}_{V_2}) + g\beta H(S^i_{Gd} + S^i_{V_1} + S^i_{V_2})\right).$$

Since the accurate calculation of the magnetic susceptibility of an infinite chain is impossible, we calculated the magnetic susceptibility of a model ring dimer composed of two {GdV_2} units of compound **1** with SH:

$$H_1^{\text{mod}} = \begin{pmatrix} -2J_1(S^1_{Gd}S^1_{V_1} + S^1_{Gd}S^1_{V_2} + S^2_{Gd}S^2_{V_1} + S^2_{Gd}S^2_{V_2}) - 2J_2(S^1_{V_1}S^2_{V_2} + S^2_{V_1}S^1_{V_2}) \\ + g\beta H(S^1_{Gd} + S^1_{V_1} + S^1_{V_2} + S^2_{Gd} + S^2_{V_1} + S^2_{V_2}) \end{pmatrix} \quad (2)$$

It should be noted that the fitting of SH (2) gives two possible sets of parameters for complex **1**:

1) J_1 (V···Gd) = 0.0071±0.0016 cm^{-1}, J_2 (V···V) = 14.7±1.3 cm^{-1}, g = 2.01

2) J_1 (V···Gd) = 0.1630±0.0075cm^{-1}, J_2 (V···V) = −1.095±0.046 cm^{-1}, g = 2.01.

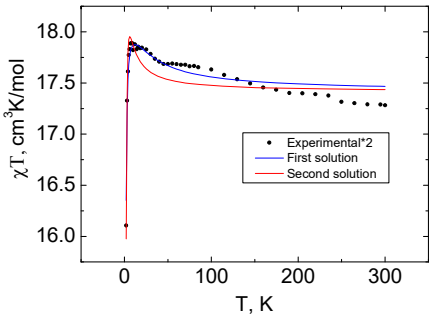

Figure S11. Temperature dependence of $\chi_M T$ for **1**. The lines represent the PHI approximations for two different solutions considering the V···V interactions.

To determine which one is correct, we studied the magnetic susceptibility of an isostructural analogue of compound **1** with diamagnetic Lu^{III} ions (**1**$_{Lu}$). Assuming that V^{IV} ions in **1**$_{Lu}$ form isolated dimers, the best agreement with experimental data is obtained with the isotropic exchange parameter $J = -0.043$ cm^{-1}, g = 2.0. Assuming that V^{IV} ions are linked in an endless chain alternately through Na and Lu^{III} ions and calculating the magnetic susceptibility of the model ring tetramer with SH

$$H_{Lu}^{\text{mod}} = \left(-2J_1(S_{V_1}^1 S_{V_2}^1 + S_{V_1}^2 S_{V_2}^2) - 2J_2(S_{V_1}^1 S_{V_2}^2 + S_{V_1}^2 S_{V_2}^1) + g\beta H(S_{V_1}^1 + S_{V_2}^1 + S_{V_1}^2 + S_{V_2}^2)\right) \quad (3)$$

we obtained J_1 (V···Gd) = −0.3478±0.0170 cm^{-1}, J_2 (V···V) = 0.4557±0.0356 cm^{-1}, g = 2.

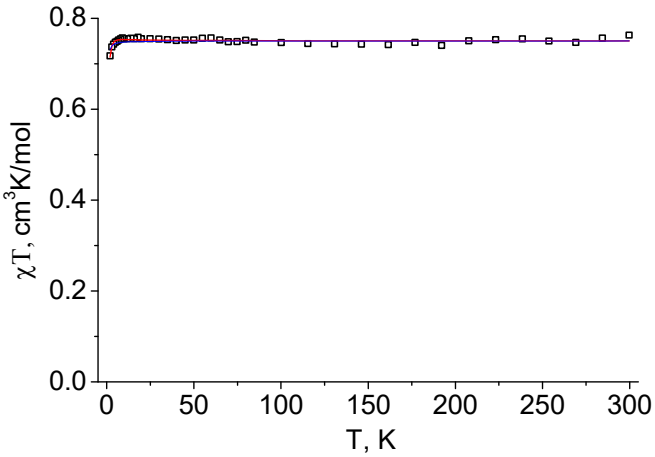

Figure S12. Experimental plot $\chi_M T$ *vs.* T for compound **1**$_{Lu}$. Blue and red lines show the values calculated for the model ring dimer and tetramer, respectively, using PHI program.

Thus, we choose the second variant of calculation for **1** with antiferromagnetic exchange between V^{IV} ions of neighboring {GdV_2} units and weak ferromagnetic exchange between V^{IV} and Gd^{III} ions: J_1= 0.1630±0.0075cm^{-1}, J_2= −1.095±0.046 cm^{-1}, g = 2.01.

AC magnetic measurements

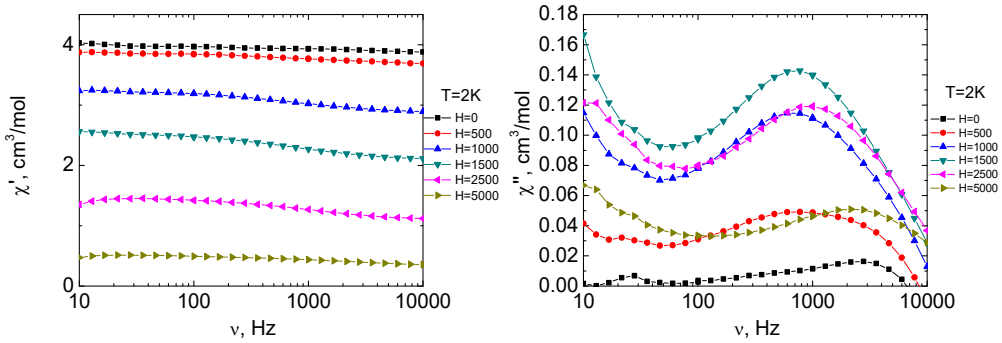

Figure S13. Frequency dependencies of real, χ' (left) and imaginary, χ'' (right) components of dynamic magnetic susceptibility for complex **1** at T = 2 K under various dc magnetic fields. Solid lines are visual guides.

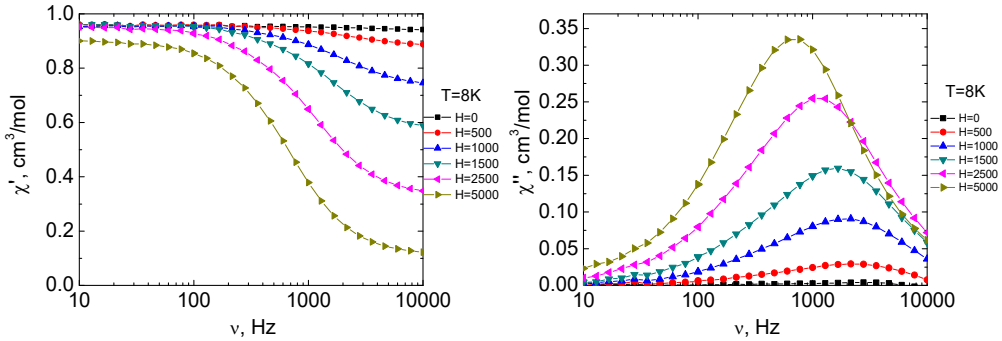

Figure S14. Frequency dependencies of real, χ' (left) and imaginary, χ'' (right) components of dynamic magnetic susceptibility for complex **1** at T = 8 K under various *dc* magnetic fields. Solid lines are visual guides.

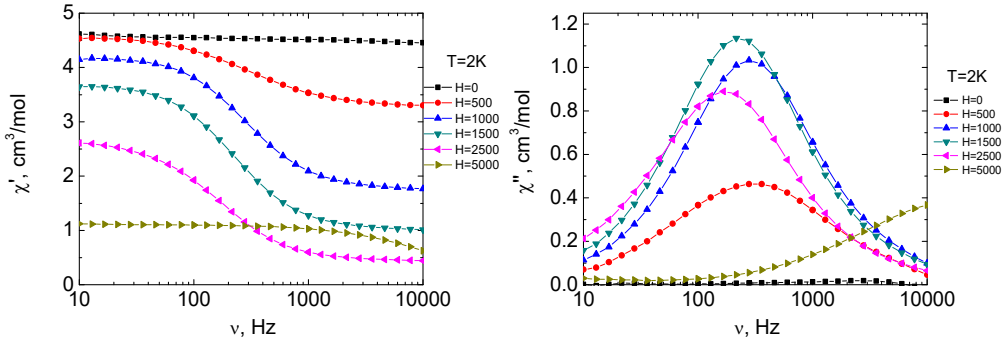

Figure S15. Frequency dependencies of real, χ' (left) and imaginary, χ'' (right) components of dynamic magnetic susceptibility for complex **2** at T = 2 K under various *dc* magnetic fields. Solid lines are visual guides.

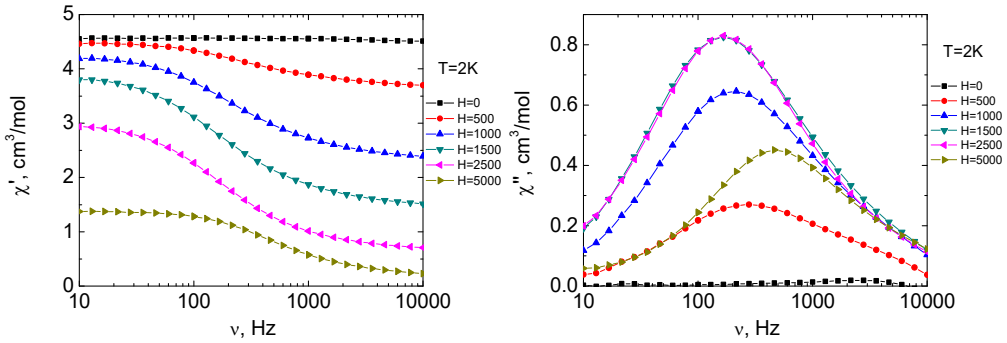

Figure S16. Frequency dependencies of real, χ' (left) and imaginary, χ'' (right) components of dynamic magnetic susceptibility for complex **3** at T = 2 K under various dc magnetic fields. Solid lines are visual guides.

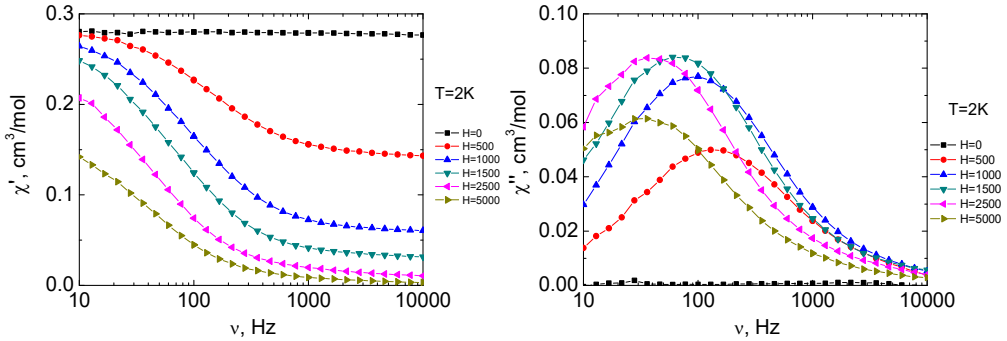

Figure S17. Frequency dependencies of real, χ' (left) and imaginary, χ'' (right) components of dynamic magnetic susceptibility for complex $\mathbf{1}_{Lu}$ at T = 2 K under various dc magnetic fields. Solid lines are visual guides.

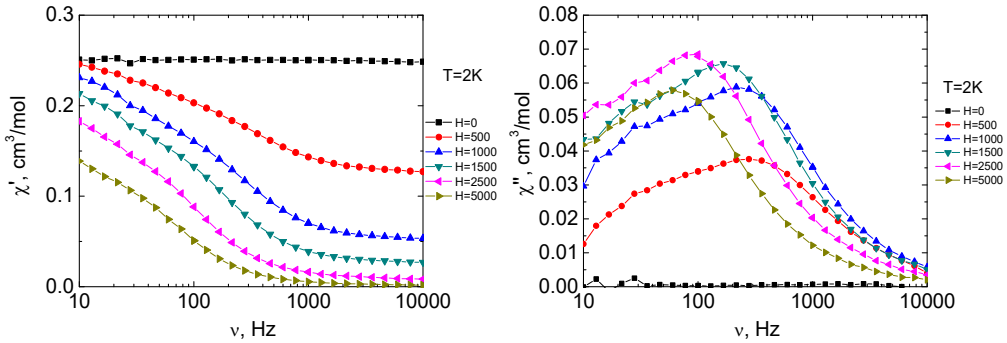

Figure S18. Frequency dependencies of real, χ' (left) and imaginary, χ'' (right) components of dynamic magnetic susceptibility for complex $\mathbf{1}_{Y}$ at T = 2 K under various dc magnetic fields. Solid lines are visual guides.

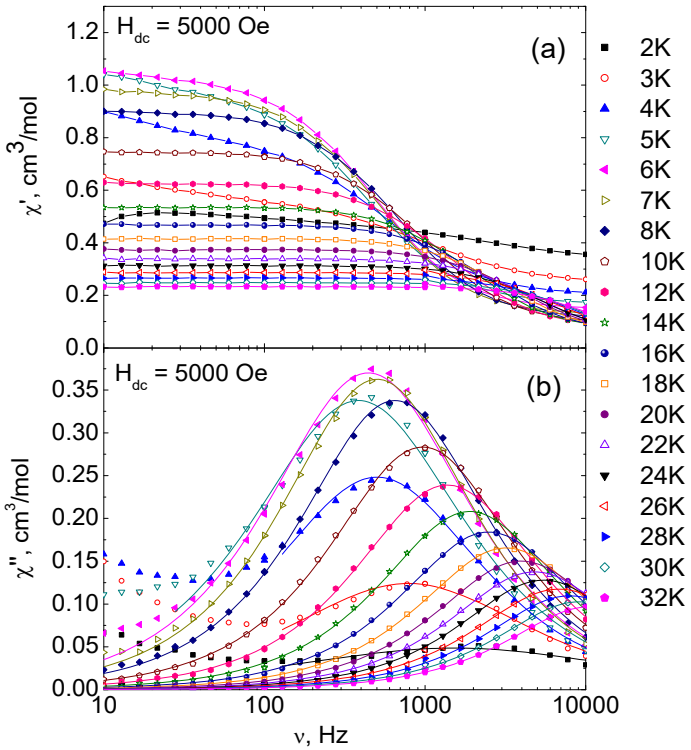

Figure S19. Frequency dependencies of the real (a) and imaginary (b) components of the ac-magnetic susceptibility for complex **1** in the 2-32 K range taken under the optimal 5000 Oe *dc*-field. Solid lines are visual guides (a), represent fitting by the generalized Debye model (b).

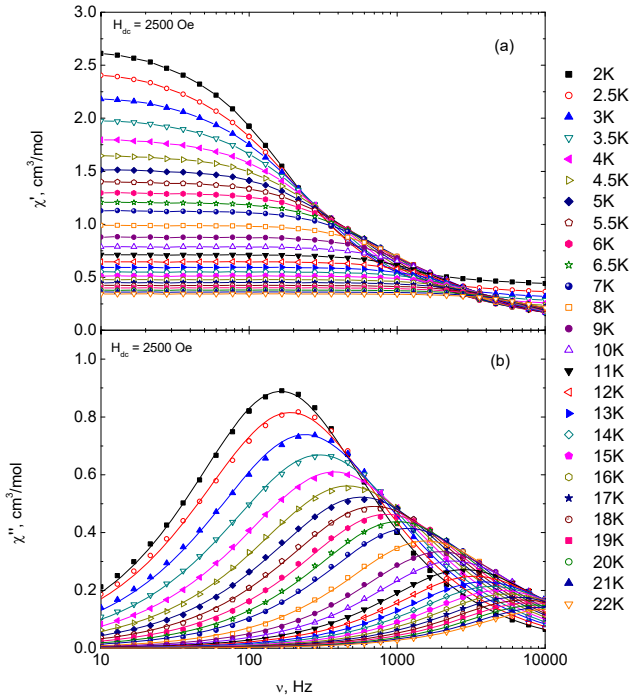

Figure S20. Frequency dependencies of the real (a) and imaginary (b) components of the *ac*-magnetic susceptibility for complex **2** in the 2-22 K range taken under the optimal 2500 Oe *dc*-field. Solid lines are visual guides (a), represent fitting by the generalized Debye model (b).

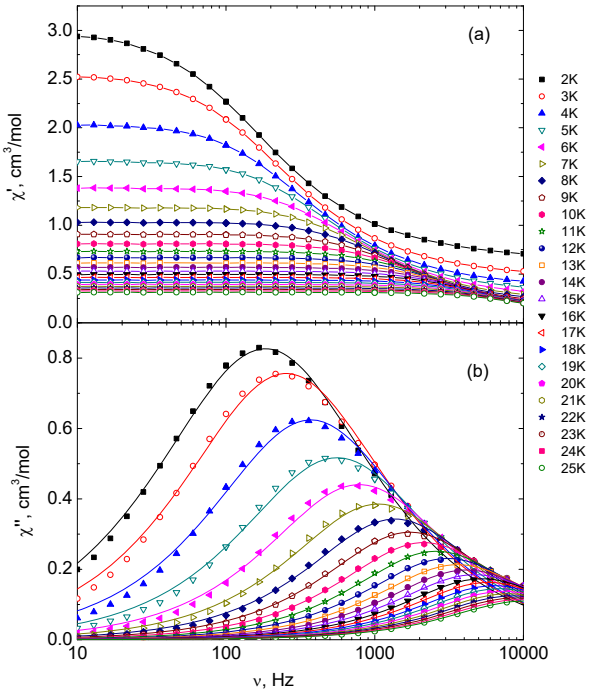

Figure S21. Frequency dependencies of the real (a) and imaginary (b) components of the *ac*-magnetic susceptibility for complex **3** in the 2-25 K range taken under the optimal 2500 Oe *dc*-field. Solid lines are visual guides (a), represent fitting by the generalized Debye model (b).

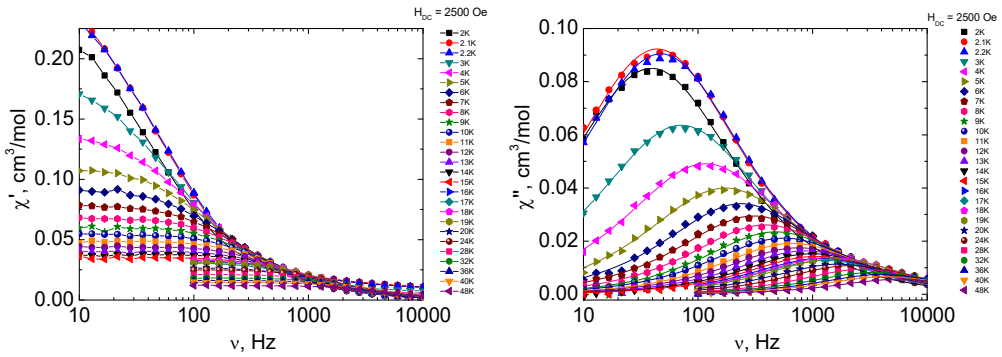

Figure S22. Frequency dependencies of the real (left) and imaginary (right) components of the *ac*-magnetic susceptibility for complex $\mathbf{1}_{Lu}$ in the 2-48 K range taken under the optimal 2500 Oe *dc*-field. Solid lines are visual guides (left), represent fitting by the generalized Debye model (right).

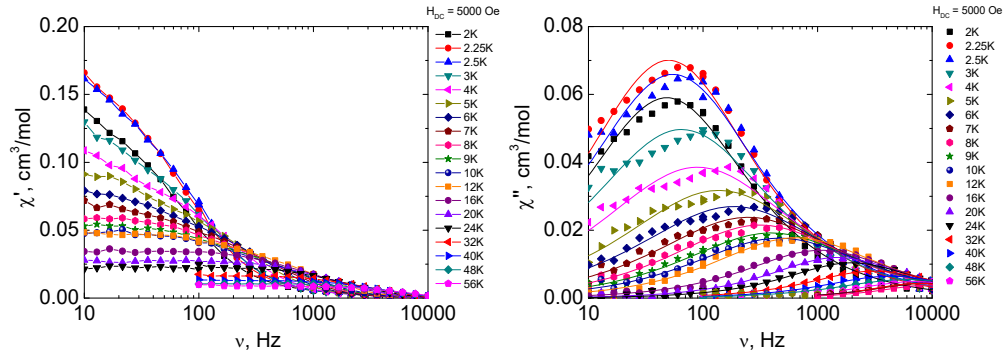

Figure S23. Frequency dependencies of the real (left) and imaginary (right) components of the *ac*-magnetic susceptibility for complex **1**Y in the 2-56 K range taken under the optimal 5000 Oe *dc*-field. Solid lines are visual guides (left), represent fitting by the generalized Debye model (right).

Table S14. Fitting of the τ *vs.* T dependences for **1**.

Dependence of the relaxation time τ on the reciprocal temperature for complex 1 (H = 5 kOe, T = 6–32 K).	**Fit function, temperature range, and the best-fit parameters with uncertainties.**
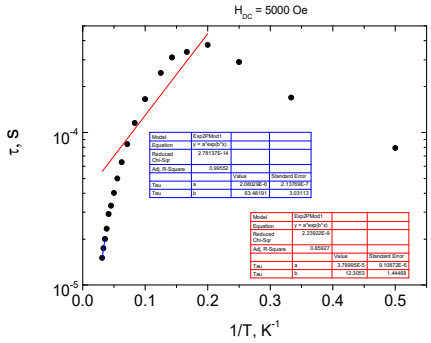	**Orbach** $\tau = \tau_0 \cdot \exp(\Delta E/kT)$ T = 28–32 K $\Delta E/k$ = 63±3 K $\tau_0 = 2.1 \cdot 10^{-6} \pm 2 \cdot 10^{-7}$ s R^2 = 0.99552 (blue line) T = 6-32 K $\Delta E/k$ = 12±1 K $\tau_0 = 3.8 \cdot 10^{-5} \pm 9 \cdot 10^{-6}$ s R^2 = 0.85927 (red line) *Unsatisfactory fit*
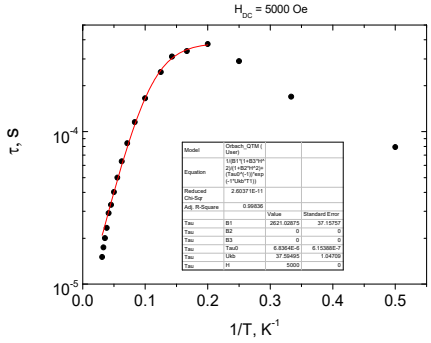	**Orbach+ QTM** $\tau^{-1} = \tau_0^{-1} \cdot \exp(-\Delta E/kT) + B$ T = 6-32 K $\Delta E/k$ = 38±1 K $\tau_0 = 6.8 \cdot 10^{-6} \pm 6 \cdot 10^{-7}$ s B= 2621± 37 s^{-1} R^2 = 0.99836
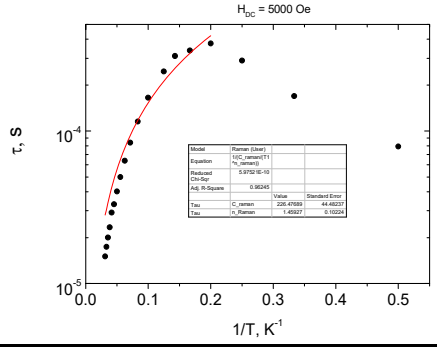	**Raman** $\tau^{-1} = C_{Raman} T^{n\_Raman}$ T = 6-32 K C_{Raman}= 226±44 $s^{-1}K^{-nRaman}$ n_{Raman}= 1.5±0.1 R^2 = 0.96245

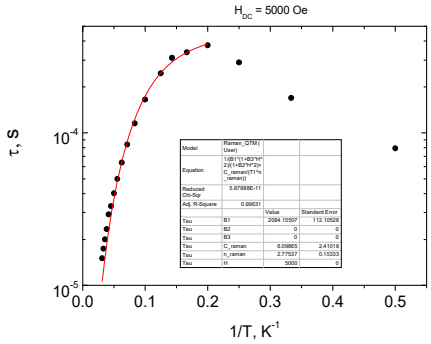

Raman+ QTM

$\tau^{-1} = C_{Raman}T^{nRaman} + B$

T = 6-32 K

C_{Raman}= 6±2 $s^{-1}K^{-nRaman}$

n_{Raman}= 2.8±0.2

B = 2084±112 s^{-1}

R^2 = 0.99631

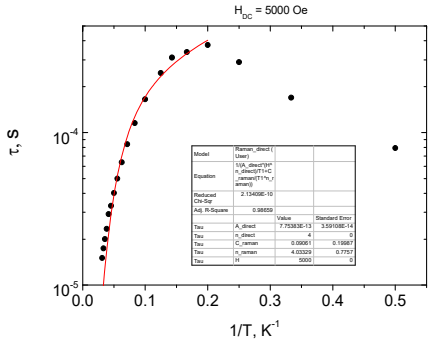

Raman+Direct

$\tau^{-1} = C_{Raman}T^{nRaman} + A_{direct}TH^4$

T = 6-32 K

C_{Raman}= 0.09±0.2 $s^{-1}K^{-nRaman}$

n_{Raman}= 4.0±0.8

A_{direct} = 7.8·10^{-13}±4·10^{-14} $K^{-1}Oe^{-4}s^{-1}$

R^2 = 0.98659

Unsatisfactory fit

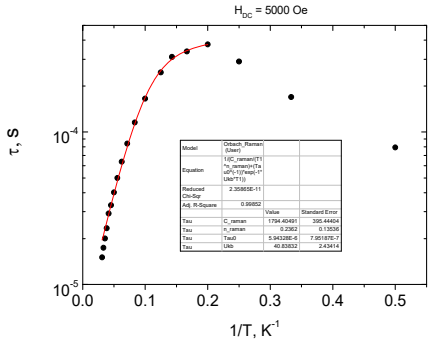

Orbach+Raman

$\tau^{-1} = \tau_0^{-1}\cdot\exp(-\Delta E/kT) + C_{Raman}T^{nRaman}$

T = 6-32 K

$\Delta E/k$ = 41±2 K

τ_0 = 5.9·10^{-6}±8·10^{-7} s

C_{Raman}= 1794±395 $s^{-1}K^{-nRaman}$

n_{Raman}= 0.2±0.1

R^2 = 0.99852

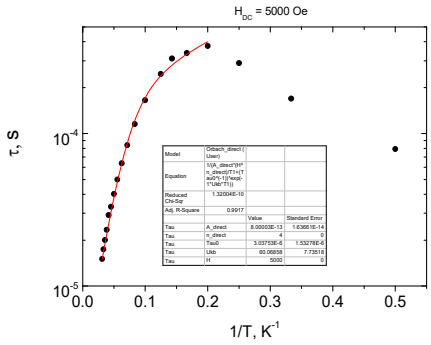

Orbach+Direct

$\tau^{-1} = \tau_0^{-1}\cdot\exp(-\Delta E/kT) + A_{direct}TH^4$

T = 6-32 K

$\Delta E/k$ = 60±8 K

τ_0 = 3·10^{-6} ±2·10^{-6} s

A_{direct} = 8.0·10^{-13}±2·10^{-14} $K^{-1}Oe^{-4}s^{-1}$

R^2 = 0.9917

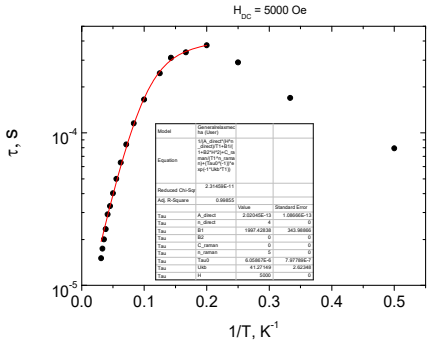	**Orbach+Direct+QTM** $\tau^{-1} = \tau_0^{-1}\cdot\exp(-\Delta E/kT)+B+A_{direct}TH^4$ T = 6-32 K $\Delta E/k$ = 41±3 K $\tau_0 = 6.1\cdot10^{-6}\pm8\cdot10^{-7}$ s $A_{direct} = 2\cdot10^{-13}\pm1\cdot10^{-13}$ $K^{-1}Oe^{-4}s^{-1}$ B = 1997±344 R^2 = 0.99855 *Over-parametrization*
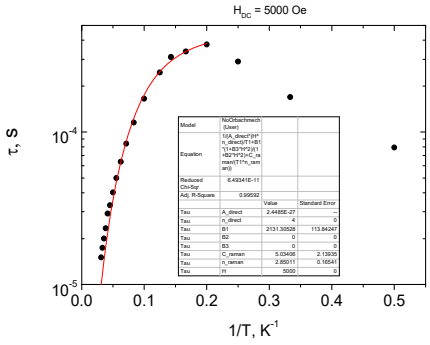	**Raman+Direct+QTM** $\tau^{-1} = C_{Raman}T^{nRaman}+B+A_{direct}TH^4$ T = 6-32 K C_{Raman}= 5±2 $s^{-1}K^{-nRaman}$ n_{Raman}= 2.9±0.2 $A_{direct} = 2\cdot10^{-27}$ $K^{-1}Oe^{-4}s^{-1}$ B = 2131±114 R^2 = 0.99592 *Unsuccessful fit*
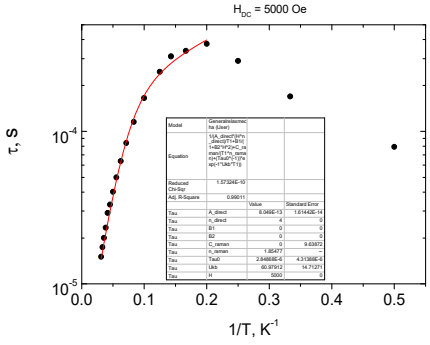	**Orbach+Raman+Direct** $\tau^{-1} = \tau_0^{-1}\cdot\exp(-\Delta E/kT)+C_{Raman}T^{nRaman}+A_{direct}TH^4$ T = 6-32 K $\Delta E/k$ = 61±15 K $\tau_0 = 3\cdot10^{-6}\pm4\cdot10^{-6}$ s C_{Raman}= 0±10 $s^{-1}K^{-nRaman}$ n_{Raman}= 1.9 $A_{direct} = 8.0\cdot10^{-13}\pm2\cdot10^{-14}$ $K^{-1}Oe^{-4}s^{-1}$ R^2 = 0.99011 *Over-parametrization* *Unsuccessful fit*
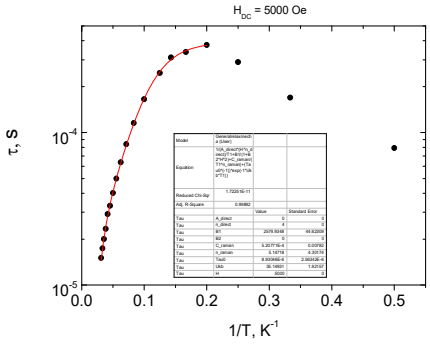	**Orbach+Raman+QTM** $\tau^{-1} = \tau_0^{-1}\cdot\exp(-\Delta E/kT)+C_{Raman}T^{nRaman}+B$ T = 6-32 K $\Delta E/k$ = 35±2 K $\tau_0 = 9\cdot10^{-6}\pm3\cdot10^{-6}$ s C_{Raman}= $5\cdot10^{-4}\pm8\cdot10^{-3}$ $s^{-1}K^{-nRaman}$ n_{Raman}= 5±4 B = 2580±45 R^2 = 0.99892 *Over-parametrization*

Table S15. Fitting of the τ *vs.* T dependences for **2**.

Dependence of the relaxation time τ on the reciprocal temperature for complex 2 (H = 2.5 kOe, T = 2–22 K).	Fit function, temperature range, and the best-fit parameters with uncertainties.
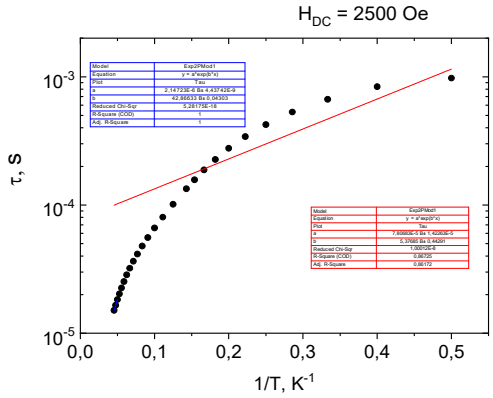	**Orbach** $\tau = \tau_0 \cdot \exp(\Delta E/kT)$ T = 20–22 K $\Delta E/k$ = 42.87±0.04 K $\tau_0 = 2.147 \cdot 10^{-6} \pm 4 \cdot 10^{-9}$ s R^2 = 1 (blue line) T = 2-22 K $\Delta E/k$ = 5.4±0.4 K $\tau_0 = 8 \cdot 10^{-5} \pm 1 \cdot 10^{-5}$ s R^2 = 0.86725 (red line) *Unsatisfactory fit*
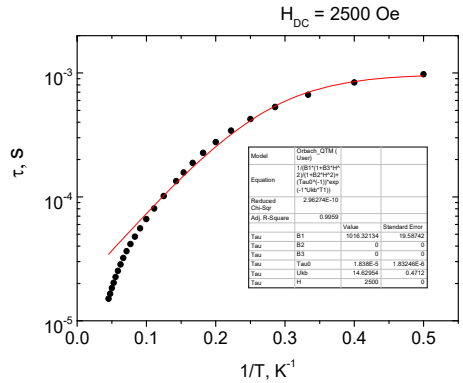	**Orbach+ QTM** $\tau^{-1} = \tau_0^{-1} \cdot \exp(-\Delta E/kT) + B$ T = 2-22 K $\Delta E/k$ = 14.6±0.5 K $\tau_0 = 1.8 \cdot 10^{-5} \pm 2 \cdot 10^{-6}$ s B= 1016± 20 s^{-1} R^2 = 0.9959
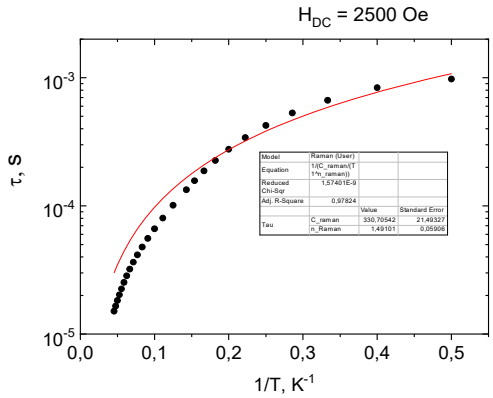	**Raman** $\tau^{-1} = C_{Raman} T^{n\_Raman}$ T = 2-22 K C_{Raman}= 331±21 $s^{-1}K^{-nRaman}$ n_{Raman}= 1.49±0.06 R^2 = 0.97824

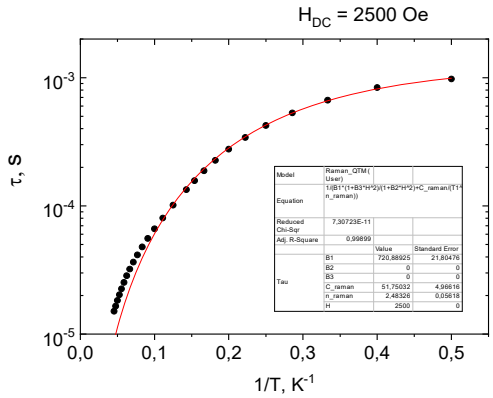

Raman+ QTM

$\tau^{-1} = C_{Raman}T^{nRaman} + B$

T = 2-22 K

C_{Raman}= 52±5 $s^{-1}K^{-nRaman}$

n_{Raman}= 2.48±0.06

B = 721±22 s^{-1}

R^2 = 0.99899

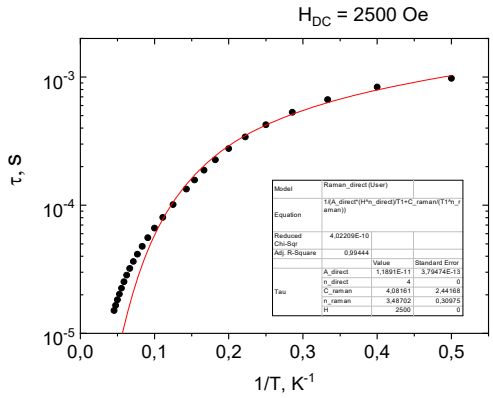

Raman+Direct

$\tau^{-1} = C_{Raman}T^{nRaman} + A_{direct}TH^4$

T = 2-22 K

C_{Raman}= 4±2 $s^{-1}K^{-nRaman}$

n_{Raman}= 3.5±0.3

A_{direct} = $1.19\cdot10^{-11}$±$4\cdot10^{-13}$ $K^{-1}Oe^{-4}s^{-1}$

R^2 = 0.99444

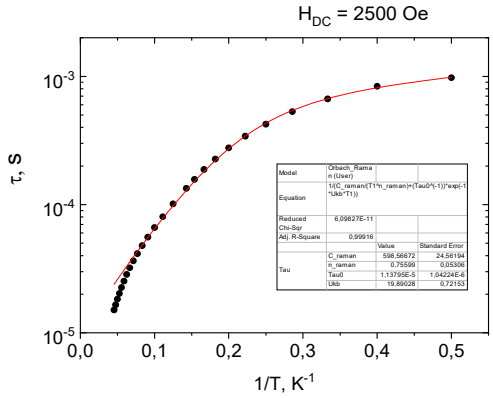

Orbach+Raman

$\tau^{-1} = \tau_0^{-1}\cdot\exp(-\Delta E/kT) + C_{Raman}T^{nRaman}$

T = 2-22 K

$\Delta E/k$ = 19.9±0.7 K

τ_0 = $1.1\cdot10^{-5}$±$1\cdot10^{-6}$ s

C_{Raman}= 599±25 $s^{-1}K^{-nRaman}$

n_{Raman}= 0.76±0.05

R^2 = 0.99916

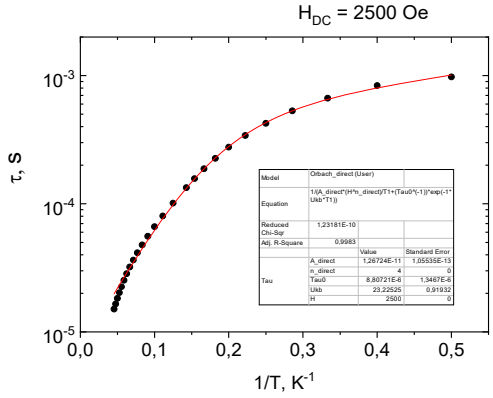

Orbach+Direct

$\tau^{-1} = \tau_0^{-1}\cdot\exp(-\Delta E/kT) + A_{direct}TH^4$

T = 2-22 K

$\Delta E/k$ = 23.2±0.9 K

τ_0 = $9\cdot10^{-6}$ ±$1\cdot10^{-6}$ s

A_{direct} = $1.27\cdot10^{-11}$±$1\cdot10^{-13}$ $K^{-1}Oe^{-4}s^{-1}$

R^2 = 0.9983

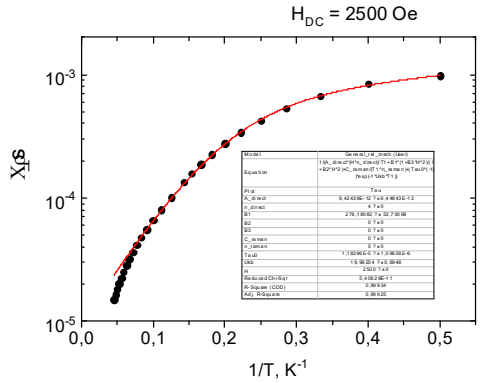

Orbach+Direct+QTM

$\tau^{-1} = \tau_0^{-1}\cdot\exp(-\Delta E/kT)+B+A_{direct}TH^4$

T = 2-22 K

$\Delta E/k$ = 20.0±0.7 K

$\tau_0 = 1.2\cdot10^{-5} \pm 1\cdot10^{-6}$ s

$A_{direct} = 9.4\cdot10^{-12} \pm 6\cdot10^{-13}$ K^{-1}Oe^{-4}s^{-1}

B = 276±58

R^2 = 0.99925

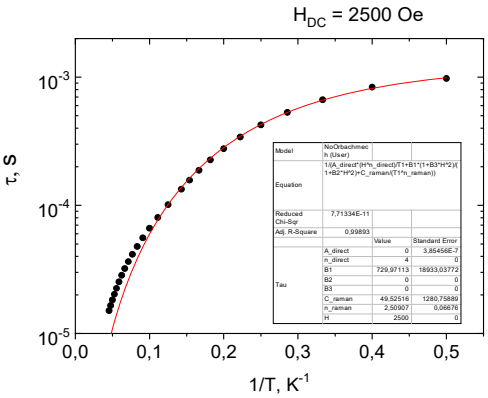

Raman+Direct+QTM

$\tau^{-1} = C_{Raman}T^{nRaman}+B+A_{direct}TH^4$

T = 2-22 K

C_{Raman}= 50±1281 s^{-1}K$^{-nRaman}$

n_{Raman}= 2.51±0.07

A_{direct} = 0 ±4·10^{-7} K^{-1}Oe^{-4}s^{-1}

B = 730±18933

R^2 = 0.99893

Over-parametrization

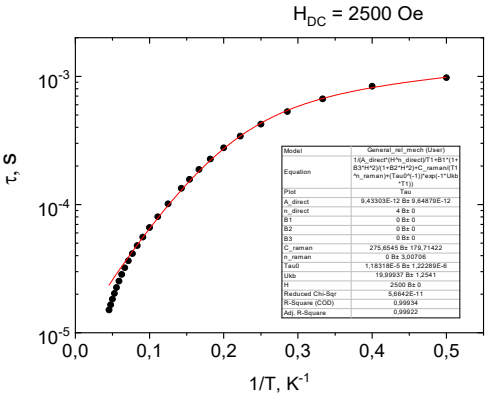

Orbach+Raraman+Direct

$\tau^{-1} = \tau_0^{-1}\cdot\exp(-\Delta E/kT)+C_{Raman}T^{nRaman}+A_{direct}TH^4$

T = 2-22 K

$\Delta E/k$ = 20±1 K

$\tau_0 = 1.2\cdot10^{-5} \pm 1\cdot10^{-6}$ s

C_{Raman}= 276±180 s^{-1}K$^{-nRaman}$

n_{Raman}= 0±3

A_{direct} = 9·10^{-12} ±9·10^{-12} K^{-1}Oe^{-4}s^{-1}

R^2 = 0.99922

Over-parametrization

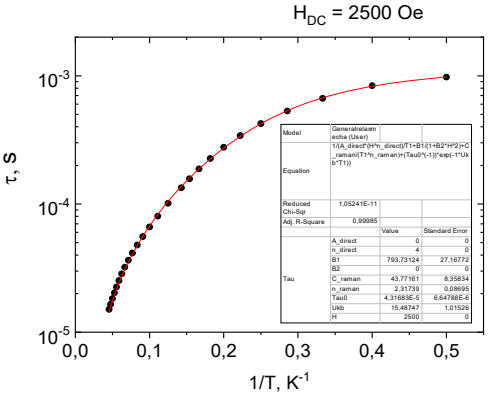

Orbach+Raman+QTM

$\tau^{-1} = \tau_0^{-1}\cdot\exp(-\Delta E/kT)+C_{Raman}T^{nRaman}+B$

T = 2-22 K

$\Delta E/k$ = 15±1 K

$\tau_0 = 4.3\cdot10^{-5} \pm 7\cdot10^{-6}$ s

C_{Raman}= 44±8 s^{-1}K$^{-nRaman}$

n_{Raman}= 2.32±0.09

B = 794±27

R^2 = 0.99985

Table S16. Fitting of the τ *vs.* T dependences for **3**.

Dependence of the relaxation time τ on the reciprocal temperature for complex 3 (H = 2.5 kOe, T = 2–25 K).	Fit function, temperature range, and the best-fit parameters with uncertainties.
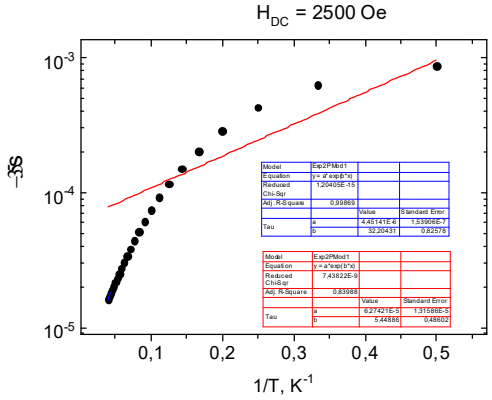	**Orbach** $\tau = \tau_0 \cdot \exp(\Delta E/kT)$ T = 23–25 K $\Delta E/k$ = 32.2±0.8 K $\tau_0 = 4.5 \cdot 10^{-6} \pm 2 \cdot 10^{-7}$ s R^2 = 0.99869 (blue line) T = 2-25 K $\Delta E/k$ = 5.4±0.5 K $\tau_0 = 6 \cdot 10^{-5} \pm 1 \cdot 10^{-5}$ s R^2 = 0.83988 (red line) *Unsatisfactory fit*
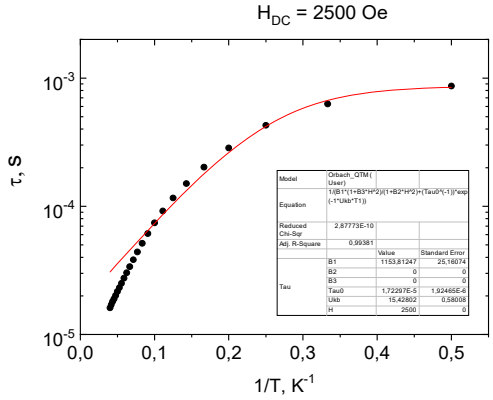	**Orbach+ QTM** $\tau^{-1} = \tau_0^{-1} \cdot \exp(-\Delta E/kT) + B$ T = 2-25 K $\Delta E/k$ = 15.4±0.6 K $\tau_0 = 1.7 \cdot 10^{-5} \pm 2 \cdot 10^{-6}$ s B= 1154± 25 s^{-1} R^2 = 0.99381
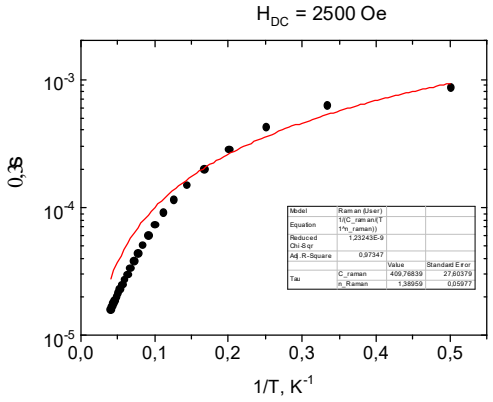	**Raman** $\tau^{-1} = C_{Raman} T^{n\_Raman}$ T = 2-25 K C_{Raman}= 410±28 $s^{-1}K^{-nRaman}$ n_{Raman}= 1.39±0.06 R^2 = 0.97347
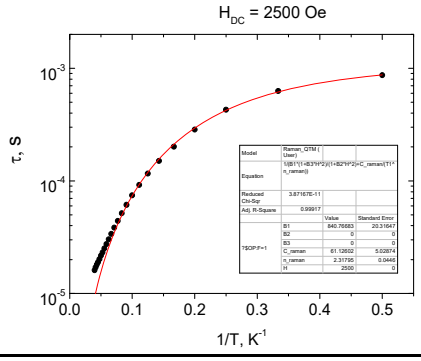	**Raman+ QTM** $\tau^{-1} = C_{Raman} T^{nRaman} + B$ T = 2-25 K C_{Raman}= 61±5 $s^{-1}K^{-nRaman}$ n_{Raman}= 2.32±0.04 B = 841±20 s^{-1} R^2 = 0.99917

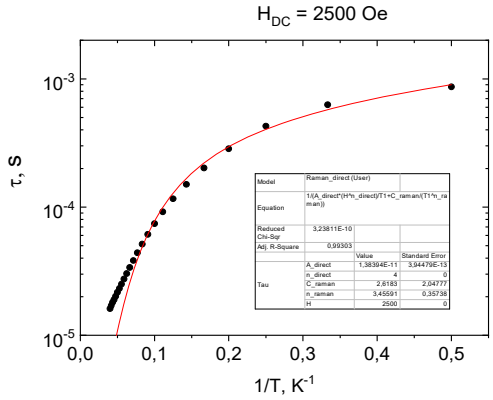

Raman+Direct

$\tau^{-1} = C_{Raman}T^{nRaman} + A_{direct}TH^4$

T = 2-25 K

C_{Raman}= 2.6±2.0 $s^{-1}K^{-nRaman}$

n_{Raman}= 3.5±0.4

A_{direct} = $1.38 \cdot 10^{-11} \pm 4 \cdot 10^{-13}$ $K^{-1}Oe^{-4}s^{-1}$

R^2 = 0.99303

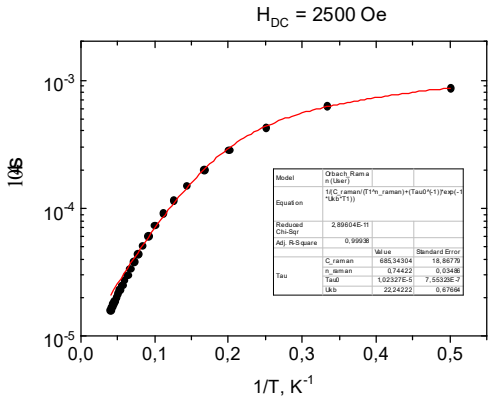

Orbach+Raman

$\tau^{-1} = \tau_0^{-1} \cdot \exp(-\Delta E/kT) + C_{Raman}T^{nRaman}$

T = 2-25 K

$\Delta E/k$ = 22.2±0.7 K

$\tau_0 = 1.02 \cdot 10^{-5} \pm 8 \cdot 10^{-7}$ s

C_{Raman}= 685±19 $s^{-1}K^{-nRaman}$

n_{Raman}= 0.74±0.03

R^2 = 0.99938

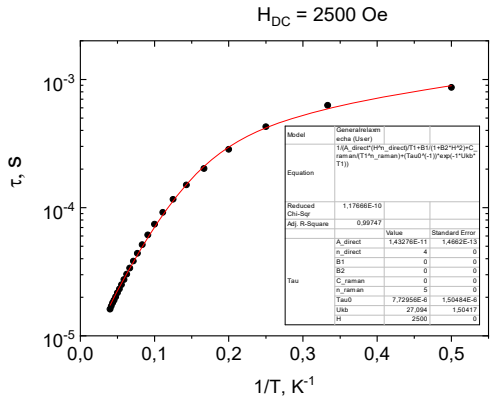

Orbach+Direct

$\tau^{-1} = \tau_0^{-1} \cdot \exp(-\Delta E/kT) + A_{direct}TH^4$

T = 2-25 K

$\Delta E/k$ = 27±2 K

$\tau_0 = 8 \cdot 10^{-6} \pm 2 \cdot 10^{-6}$ s

A_{direct} = $1.43 \cdot 10^{-11} \pm 1 \cdot 10^{-13}$ $K^{-1}Oe^{-4}s^{-1}$

R^2 = 0.99747

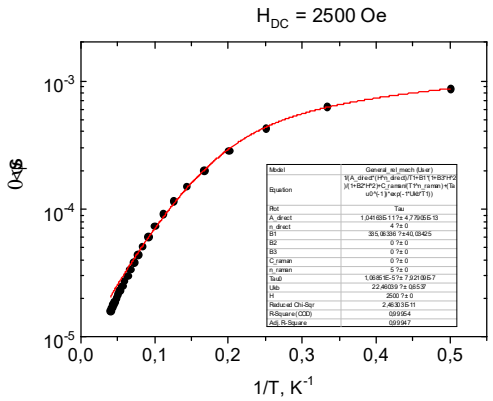

Orbach+Direct+QTM

$\tau^{-1} = \tau_0^{-1} \cdot \exp(-\Delta E/kT) + B + A_{direct}TH^4$

T = 2-25 K

$\Delta E/k$ = 22.5±0.7 K

$\tau_0 = 1.07 \cdot 10^{-5} \pm 8 \cdot 10^{-7}$ s

A_{direct} = $1.04 \cdot 10^{-11} \pm 5 \cdot 10^{-13}$ $K^{-1}Oe^{-4}s^{-1}$

B = 335±40

R^2 = 0.99947

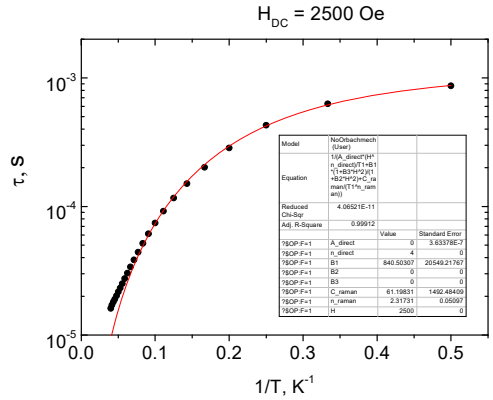

Raman+Direct+QTM

$\tau^{-1} = C_{Raman}T^{nRaman}+B+A_{direct}TH^4$

T = 2-25 K

C_{Raman}= 61±1492 $s^{-1}K^{-nRaman}$

n_{Raman}= 2.32±0.05

A_{direct} = 0±4·10^{-7} $K^{-1}Oe^{-4}s^{-1}$

B = 841±20549

R^2 = 0.99912

Over-parametrization

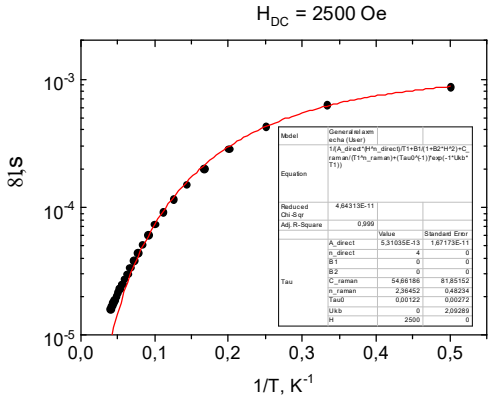

Orbach+Raman+Direct

$\tau^{-1} = \tau_0^{-1}\cdot\exp(-\Delta E/kT)+C_{Raman}T^{nRaman}+A_{direct}TH^4$

T = 2-25 K

$\Delta E/k$ = 0±2 K

τ_0 = 0.001 ±0.003 s

C_{Raman}= 55±82 $s^{-1}K^{-nRaman}$

n_{Raman}= 2.4±0.5

A_{direct} = 5·10^{-13} ±2·10^{-11} $K^{-1}Oe^{-4}s^{-1}$

R^2 = 0.999

Over-parametrization

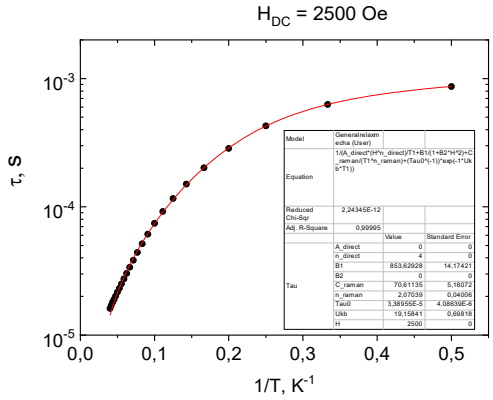

Orbach+Raman+QTM

$\tau^{-1} = \tau_0^{-1}\cdot\exp(-\Delta E/kT)+C_{Raman}T^{nRaman}+B$

T = 2-25 K

$\Delta E/k$ = 19.2±0.7 K

τ_0 = 3.4·10^{-5} ±4·10^{-6} s

C_{Raman}= 71±5 $s^{-1}K^{-nRaman}$

n_{Raman}= 2.07±0.04

B = 854±14

R^2 = 0.99995

S-IV. DFT calculations

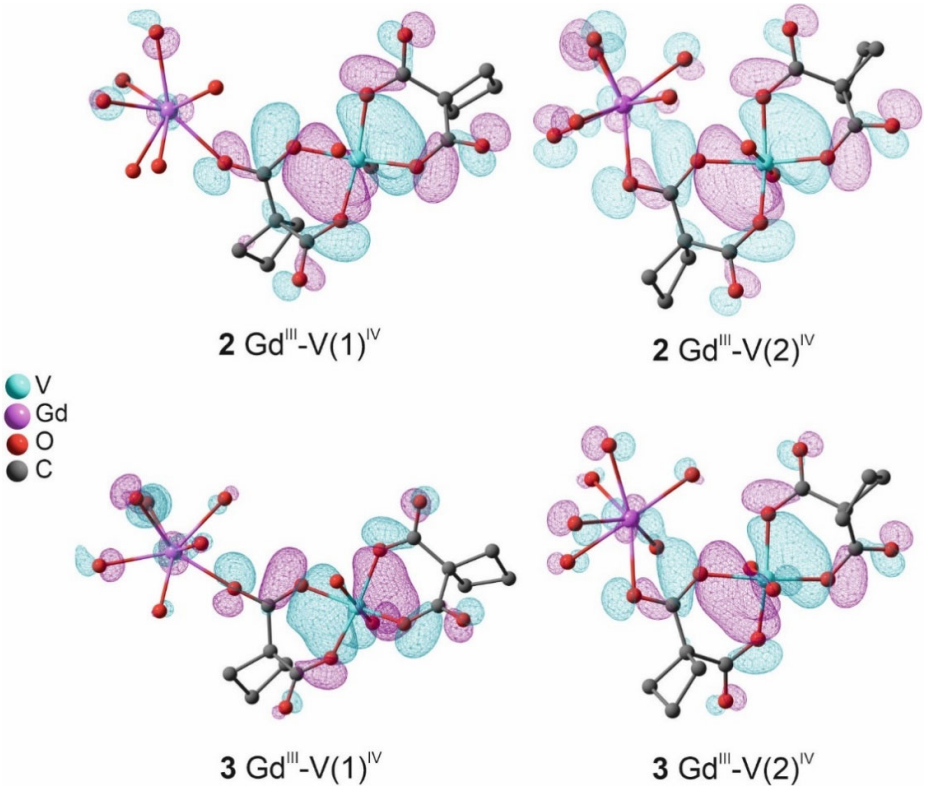

Figure S24. Natural orbitals of V^{IV}-Gd^{III} fragments of the compounds **2** and **3** calculated by the DFT UB3LYP/6-31G(d,p)/SDD with inclusion of relativistic effects *via* the Douglas–Kroll–Hess method. Hydrogen atoms are omitted, cutoff = 0.015 e/Å^3.

S-V. Powder X-ray Diffraction

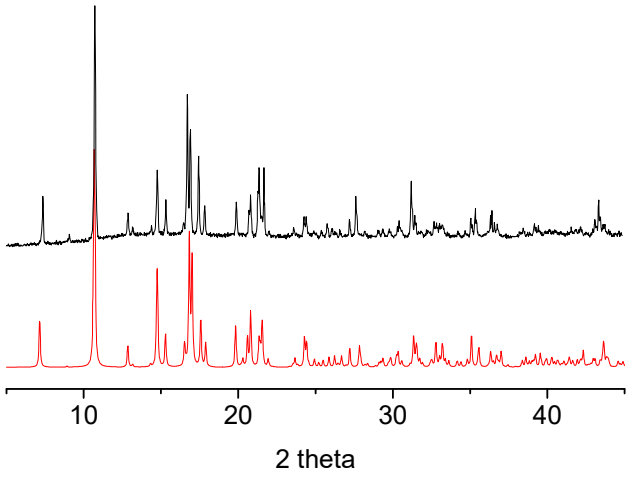

Figure S25. Experimental PXRD pattern for **1** measured at 273 K (black line) and its comparison with calculated data (red line).

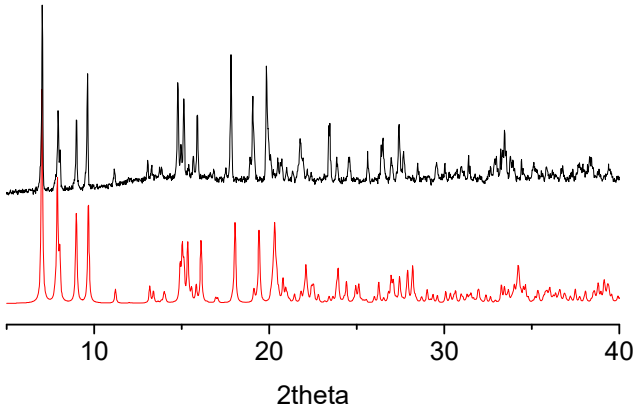

Figure S26. Experimental PXRD pattern for **2** measured at 273 K (black line) and its comparison with calculated data (red line).

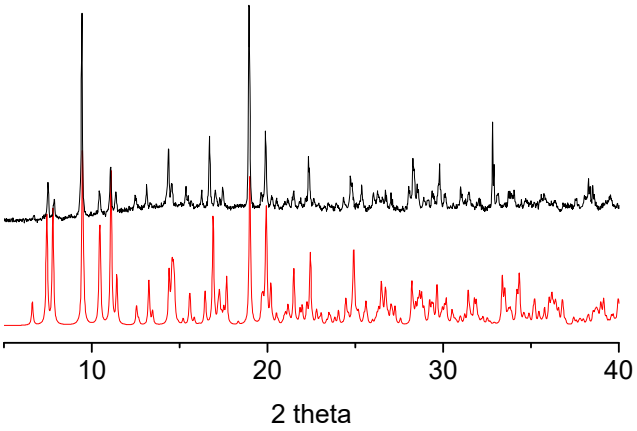

Figure S27. Experimental PXRD pattern for **3** measured at 273 K (black line) and its comparison with calculated data (red line).

References

S1.→ Kurganskii, I.V.; Bazhina, E.S.; Korlyukov, A.A.; Babeshkin, K.A.; Efimov, N.N.; Kiskin, M.A.; Veber, S.L.; Sidorov, A.A.; Eremenko, I.L.; Fedin, M.V. Mapping Magnetic Properties and Relaxation in Vanadium(IV) Complexes with Lanthanides by Electron Paramagnetic Resonance. *Molecules* **2019**, *24*, 4582.

S2.→ Chilton, N.F.; Anderson, R.P.; Turner, L.D.; Soncini, A.; Murray, K.S. PHI: a powerful new program for the analysis of anisotropic monomeric and exchange-coupled polynuclear d- and f-block complexes. *J. Comput. Chem*. **2013**, *34*, 1164.